

1 **Title:** Three decades of Landsat-derived spring surface water dynamics in an agricultural
2 wetland mosaic; implications for migratory shorebirds

3

4 **Author names and affiliations:**

5 Danica Schaffer-Smith^{a*}

6 Jennifer J. Swenson^a

7 Blake Barbaree^b

8 Matthew E. Reiter^b

9 ^aNicholas School of the Environment, Duke University, Durham NC, 27708, USA.

10 ^bPoint Blue Conservation Science, Petaluma, CA, 94954, USA.

11 *Corresponding author at: Nicholas School of the Environment, Duke University, Box 90328,
12 Durham NC, 27708, USA.

13 Email address: danica.schaffer.smith@duke.edu

14

15

16 **Abstract:**

17 Satellite measurements of surface water offer promise for understanding wetland habitat
18 availability at broad spatial and temporal scales; reliable habitat is crucial for the persistence of
19 migratory shorebirds that depend on wetland networks. We analyzed water extent dynamics
20 within wetland habitats at a globally important shorebird stopover site for a 1983-2015 Landsat
21 time series, and evaluated the effect of climate on water extent. A range of methods can detect
22 open water from imagery, including supervised classification approaches and thresholds for
23 spectral bands and indices. Thresholds provide a time advantage; however, there is no
24 universally superior index, nor single best threshold for all instances. We used random forest to
25 model the presence or absence of water from >6,200 reference pixels, and derived an optimal
26 water probability threshold for our study area using receiver operating characteristic curves. An
27 optimized mid-infrared (1.5–1.7 μm) threshold identified open water in the Sacramento Valley
28 of California at 30-m resolution with an average of 90% producer's accuracy, comparable to
29 approaches that require more intensive user input. SLC-off Landsat 7 imagery was integrated by
30 applying a customized interpolation that mapped water in missing data gaps with 99% user's
31 accuracy. On average we detected open water on ~26,000 ha (~3% of the study area) in early
32 April at the peak of shorebird migration, while water extent increased five-fold after the
33 migration rush. Over the last three decades, late March water extent declined by ~1,300 ha per
34 year, primarily due to changes in the extent and timing of agricultural flood-irrigation. Water
35 within shorebird habitats was significantly associated with an index of water availability at the
36 peak of migration. Our approach can be used to optimize thresholds for time series analysis and
37 near-real-time mapping in other regions, and requires only marginally more time than generating
38 a confusion matrix.

40 **1. Introduction**

41 Freshwater resources provide benefits to human and natural communities ranging from
42 water, food and habitat provision, to waste treatment and greenhouse gas regulation; yet these
43 critical resources are limited to <1% of the Earth's surface. Despite this small areal extent, there
44 are substantial gaps in our knowledge of the distribution and variability of terrestrial surface
45 water resources over time (Alsdorf, et al., 2007; Turpie et al., 2015). Freshwater is poorly
46 monitored and managed across the globe, especially with regard to wetlands and water applied to
47 agricultural lands (Alsdorf et al., 2007; Pimentel et al., 2004). Even in California, which has one
48 of the most highly engineered and intensively managed water systems in the U.S., water rights in
49 some areas represent 1,000% of the surface water supply (Grantham & Viers, 2014; Jenkins et
50 al., 2004). Recent pronounced droughts highlight the added complexity of management under
51 climate change interacting with human-imposed water stress, particularly in arid regions with
52 high rates of wetland conversion (Maggioni, 2015; Van Loon et al., 2016).

53 Over half of the 75 shorebird species in the Western Hemisphere are in decline (Brown,
54 Hickey, Harrington, & Gill, 2001), indicating that wetland networks are in peril. Most migratory
55 shorebird species are entirely dependent on wetlands for food and rest during long-distance
56 journeys in the spring and fall (Brown et al., 2001); many face dual threats of habitat loss and
57 climate change (Davidson, 2014; Morrison et al., 2006). Under ongoing climate change, inland
58 non-tidal wetlands are at increased risk from future drought severity, and they will increase in
59 importance for migratory shorebirds when sea level rise reduces access to coastal wetlands
60 (Galbraith et al., 2002; Werner, et al., 2013). To safeguard migratory flyways into the future,
61 improved understanding of long-term wetland extent and variability over large areas is needed,

62 as well as insight into the capacity for these systems to tolerate changes in water availability
63 (Dudgeon et al., 2005; Turpie et al., 2015).

64 Satellite remote sensing is key to understanding surface water resources and how they are
65 responding to intensified appropriation and modification by humans (Alsdorf et al., 2007; Turpie
66 et al., 2015). In recent years, several global inundation analyses have been released that have
67 moved from static, coarse scale (>1 km) products (e.g., Bontemps et al., 2011; Lehner & Döll,
68 2004; Verpoorter, et al., 2014) to more dynamic offerings, such as the Global Inundation Extent
69 from Multi-Satellites (Fluet-Chouinard, et al., 2015) and the MODIS water mask (Carroll et al.
70 2009). Studies of wetland dynamics at global scales have typically focused on relatively short
71 time periods with coarse spatial resolution (e.g., Papa et al., 2010; Prigent, et al., 2007; 25-km
72 grid cells), and therefore have been unable to capture smaller wetland features, or account for
73 longer term cyclical hydrologic variability.

74 Landsat Thematic Mapper imagery can be used to map open water at 30-m resolution
75 (Alsdorf et al., 2007; Baker, et al., 2006) appropriate for resolving smaller, shallow wetlands that
76 provide important migratory shorebird habitat (Strum et al., 2013). There is great potential for
77 tracking long-term surface water dynamics given Landsat's <16-day revisit period from 1983 to
78 the present (e.g., Feng, et al., 2016; Mueller et al., 2016; Tulbure, et al., 2016). The presence and
79 duration of flooding can be informative in lieu of more intensive field measurements (Elphick,
80 2008; Farmer & Parent, 1997; Reiter et al., 2015). For example, these attributes influence
81 invertebrate prey densities, which are challenging to measure precisely in situ over large areas
82 (Batzer, 2013; Lee, et al., 1999; Lyzenga, et al., 2006). Landsat's historical timespan permits
83 analysis of multiple El Niño cycles, which strongly influence the frequency and intensity of
84 precipitation for many regions, including the western U.S. (Feldl & Roe, 2011; Hurrell & Loon,

85 1997). An analysis of the spatiotemporal variability of surface water at migratory stopover sites
86 is needed to better understand baseline habitat conditions, particularly in regions with extreme
87 seasonal and interannual variability.

88 Various approaches to identify surface water based on satellite imagery have been
89 developed. Unsupervised classification approaches have been the most common technique in the
90 past for mapping wetlands (Ozesmi & Bauer, 2002). Of the many supervised classification
91 methods available, maximum likelihood has been used most frequently (Mather, 1985; Ozesmi
92 & Bauer, 2002), however classification trees have become increasingly popular, and typically
93 produce superior results (Baker et al., 2006; Breiman, 2001; Friedl & Brodley, 1997; Tulbure &
94 Broich, 2013). Thresholds can also be used for land cover mapping, with an advantage of lower
95 overall investment for the user; once developed, a classification can be generated virtually
96 instantaneously (Chuvieco, 2016; Friedl & Brodley, 1997). Thresholds can be identified from
97 individual multi-spectral bands as well as water indices such as the normalized difference water
98 index (NDWI; McFeeters, 1996), modified normalized difference water index (MNDWI; Xu,
99 2006), automated water extraction index (AWEI; Feyisa, et al., 2014) and Tasseled Cap wetness
100 index (Crist & Cicone, 1984).

101 These water indices have variable performance depending on scene conditions and study
102 area extent (Fisher, et al., 2016; Yang et al., 2015); thresholds also vary in time and space (Friedl
103 & Brodley, 1997). Thorough comparisons of multiple indices have been limited to a handful of
104 studies (Campos, et al., 2012; Fisher et al., 2016; Ji, et al., 2009) with no clear best index for
105 global application. Previous research indicates that thresholds should be modified for local
106 conditions (Feyisa et al., 2014; Xu, 2006), yet few studies provide guidance for appropriate
107 threshold optimization methods. A recent study by Campos et al., 2012 used the mean and

108 standard deviation of values across 12 monthly images to select a threshold, while others have
109 used omission and commission error as the basis of threshold selection (Fisher et al., 2016; Yang
110 et al., 2015). Sheng et al. (2016) used iterative segmentation to identify NDWI thresholds for
111 mapping lakes in Oceania. Ji et al. (2009) used spectral unmixing of pure pixels derived in a lab
112 setting to suggest default thresholds for different fractional water coverages (starting points for
113 25, 50, 75, 100% water cover). Some of these studies remain untested outside of lab conditions
114 (Ji et al., 2009), while others incorporate more field validation points than is normally practical
115 (Fisher et al., 2016). Most studies do not explicitly evaluate accuracy outside of the source
116 regions and dates used to train water classifications (Campos et al., 2012; Feyisa et al., 2014;
117 Fisher et al., 2016; Sheng et al., 2016), which is of particular import for time series analysis.

118 This study used the entire Landsat thematic mapper time series (1983-2015) to evaluate
119 water distribution patterns during spring shorebird migration in the Sacramento Valley of
120 California, a globally important wetland stopover (Western Hemisphere Shorebird Reserve
121 Network, 2009). Previously published water mapping work in this system over shorter timescales
122 (<10 years) has employed Landsat in both unsupervised and supervised classifications (Reiter et
123 al., 2015; Reiter & Liu, 2011; Spell, et al., 1995). Classification and change detection procedures
124 must be efficient if applied across an extensive time series, and retain a satisfactory level of
125 accuracy. Our objectives were to: 1) develop a reproducible approach to optimize a threshold
126 that accurately identifies open water from the Landsat surface reflectance time series, 2) compare
127 this approach to other methods typically used in mapping water, and 3) assess spatial and
128 temporal patterns of open water from the historical record to inform water and wetland
129 management. Hereafter we use *water* to refer to areas where open water, unobscured by
130 vegetation, was present and *non-water* to refer to regions where open water was not detected.

131

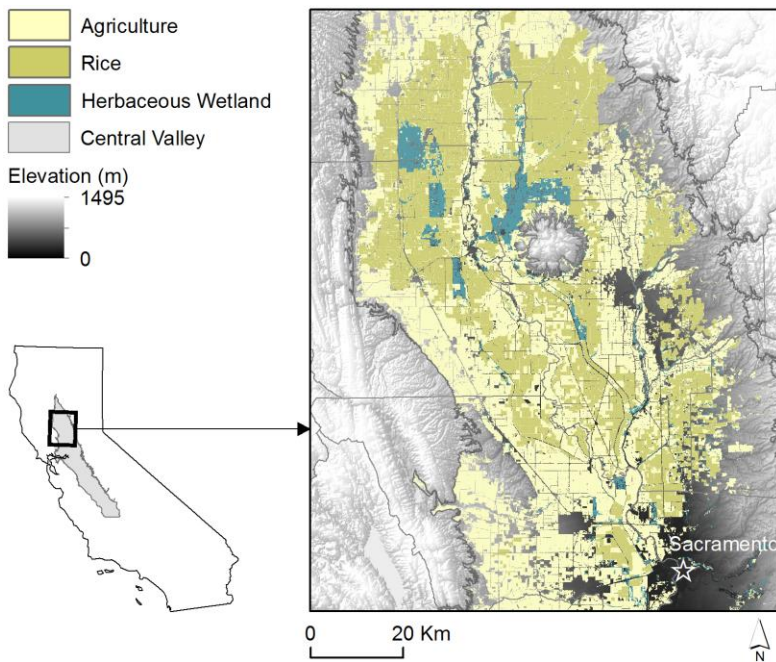
132 **2. Data and Methods**

133 We first built a Landsat surface reflectance time series for cloud-free, non-urban areas from
134 1983-2015. We then tested different spectral and water index thresholds against supervised
135 classification methods, and subsequently identified an overall spring water/non-water threshold
136 using extensive reference data for validation. Finally, we applied the optimized spring threshold
137 for classification of open water from the 32-year time series, and analyzed spatiotemporal
138 patterns and climate sensitivity of water within important migratory shorebird habitat.

139 **2.1. Study area**

140 The Sacramento Valley, in the northern Central Valley of California, is predominantly an
141 agricultural landscape, although highly managed herbaceous wetlands remain on federal, state,
142 and private lands (USDA-NASS, 2014; Fig. 1). More than 90% of the historically occurring
143 wetlands have been lost in the Central Valley (Frayer, et al., 1989). The Sacramento Valley hosts
144 96% of California's flood-irrigated rice (~20% of U.S production, Central Valley Joint Venture,
145 2006; Strum et al., 2013), which serves as important surrogate habitat for shorebirds in areas
146 with high wetland loss (Barbaree, et al., 2015; Elphick, 2000, 2010). Despite extensive historical
147 wetland loss, the Sacramento Valley is recognized by the Western Hemisphere Shorebird
148 Reserve Network as a site of international importance (Western Hemisphere Shorebird Reserve
149 Network, 2009). The valley provides habitat for over 400,000 shorebirds each spring, with the
150 peak of migration typically occurring in April (Central Valley Joint Venture, 2006; Shuford, et
151 al., 1998).

152 Much of California's water is supplied by the snowpack in the Sierra Nevada mountains,
153 which is projected to decrease in average volume and duration in the future (Cayan, 1996;
154 Cayan, et al., 2008). The Sacramento Valley receives an annual average of 890 mm of
155 precipitation, with the majority of accumulation from late fall through early spring (NOAA
156 National Centers for Environmental Information, 2016); however this varies with climate cycles.
157 A total of 1,488 mm of precipitation were recorded under strong El Niño conditions in 1998,
158 while only 541 mm were recorded for 2014, the third driest year on record in the state. Local
159 allocations and water application in the Central Valley are driven by water rights and policy
160 decisions, as opposed to the natural patterns of water distribution and abundance (Grantham &
161 Viers, 2014). During spring, water used in the Sacramento Valley is primarily sourced from
162 reservoirs that capture montane snowmelt and runoff, which is delivered to wetlands and
163 agricultural fields hundreds of kilometers away through an extensive network of canals, pump
164 stations and levees.



165

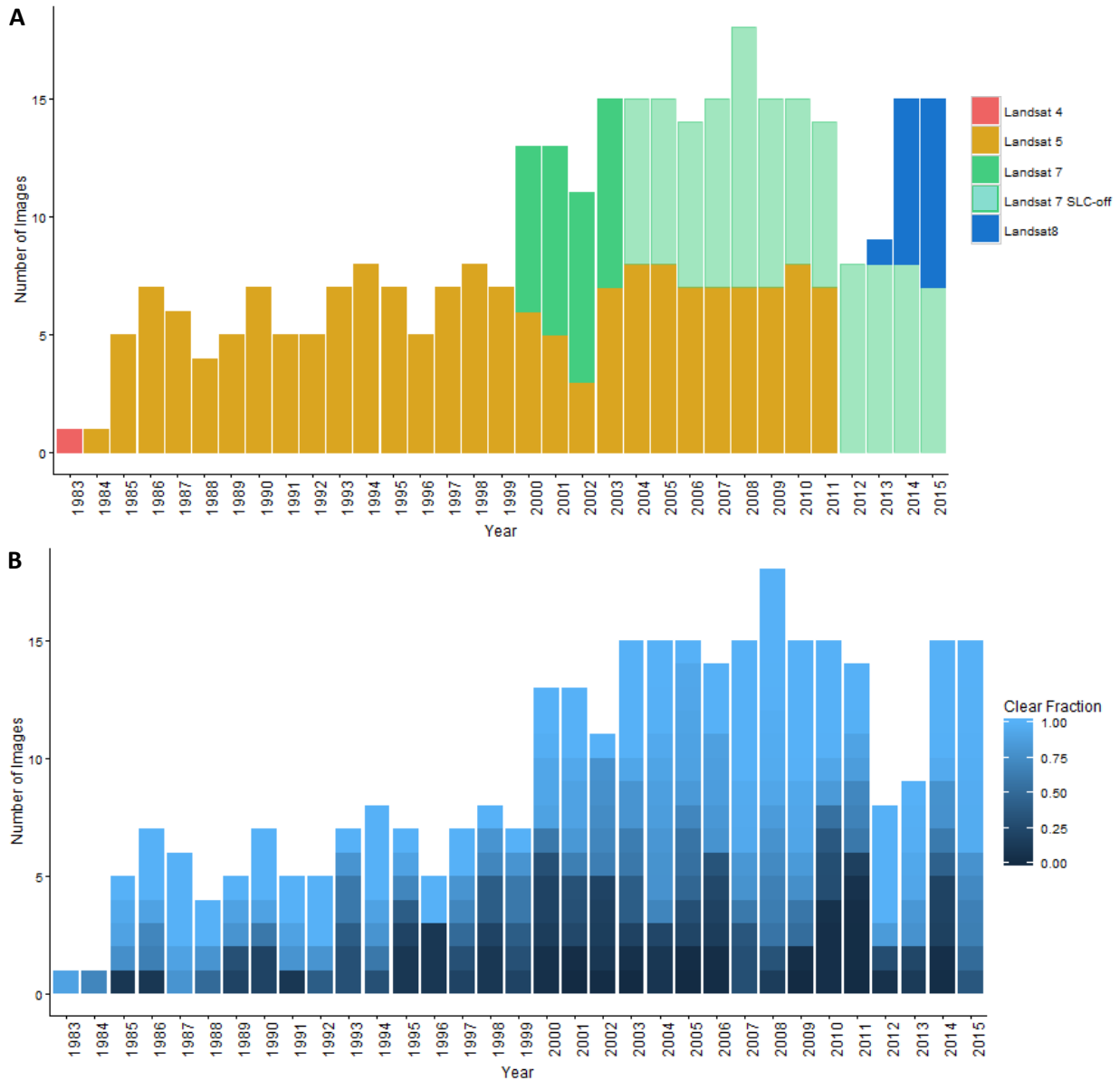
166 **Fig. 1.** Land use and land cover in the Sacramento Valley, within California’s Central Valley. (Herbaceous wetlands
167 and agriculture: National Land Cover Database (Homer et al., 2015); flood-irrigated rice: (USDA-NASS, 2014).

168 ***2.1. Analysis Tools***

169 We used the RStoolbox package in R to develop image classifications and for accuracy
170 assessment (Leutner & Horning, 2016). ArcGIS 10.3 was used to generate validation datasets,
171 and Python was used for image processing (ESRI, 2014). Modelling and statistical analysis were
172 conducted in R using the following packages: ggplot2 (Wickham, 2009), dplyr (Wickham &
173 Francois, 2015), rasterVis (Lamigueiro & Hijmans, 2016), randomForest (Liaw & Wiener,
174 2002), reshape2 (Wickham, 2007), ROCR (Sing, et al., 2005), SDMTools (VanDerWal, et al.,
175 2014), and spatial.tools (Greenberg, 2014).

176 ***2.2. Landsat time series***

177 We gathered all available Landsat surface reflectance data for the Sacramento Valley
178 representing the spring migration period (February – May) from 1983 – 2015 (WRS-2 path/row
179 44/33). Surface reflectance data were downloaded from USGS/EROS (<https://espa.cr.usgs.gov/>);
180 these images were calibrated using the LEDAPS algorithm (Landsat 4-5, 7; Masek, et al., 2013),
181 or the L8SR algorithm (Landsat 8; Vermote, et al., 2016) and CFmask (Zhu & Woodcock, 2012).
182 For the spring migration season from 1983 – 2015, we processed a total of 242 Landsat surface
183 reflectance scenes from Landsat 4, 5, 7 and 8 (Fig. 2A). These scenes had a range of cloud cover
184 (Fig. 2B), but only isolated portions of the study area were consistently affected (Fig. S1).



185

186 **Fig. 2.** Landsat surface reflectance data availability (A) and quality (clear fraction identified by the CFmask surface
 187 reflectance product) (B) for the Sacramento Valley (WRS-2 path 44/row 33) from February to May, 1983-2015.

188 **2.3. Comparison of methods to identify water vs. non-water**

189 We tested multiple methods to identify water in the study area. We used supervised
 190 maximum likelihood and random forest approaches, as well as optimized and default thresholds
 191 for commonly used water indices. To compare across both binary classifications and multi-class
 192 approaches, we generated a polygon validation dataset from a May 4, 2008 Landsat 5 image

193 acquired under clear atmospheric conditions, using synchronous Quickbird imagery as a
194 reference. We delineated polygons representing five land cover categories: open water, forested,
195 other green vegetation, dry vegetation, or barren/urban, also coding each polygon as water or
196 non-water. The open water polygons that we digitized did not include edge vegetation, but these
197 did incorporate a mix of shallow and deep water pixels. Training and testing points were sampled
198 from the polygon regions using a two-stage method after Wegmann, et al. (2015). First, we
199 partitioned the polygon dataset such that approximately 70% of the polygons were used for
200 model training and 30% for model testing, in order to maximize spatial independence. For model
201 training, we randomly sampled 500 points drawn from each class of interest (either water/non-
202 water or multiple land cover types) in the training polygon set, removing points drawn from
203 duplicate cells. We assessed the final water/non-water classifications produced by each approach
204 using independent confirmed water and non-water locations; 250 points in each class were
205 sampled from the May 4, 2008 Quickbird polygon testing regions and filtered to remove
206 duplicates.

207 Supervised maximum likelihood and random forest (10,000 trees, mtry = 1)
208 classifications were used to map five cover types: water (490 training points), forested (453
209 training points), other green vegetation (418 training points), dry vegetation (460 training points)
210 and urban/barren (434 training points). For both supervised methods, the resulting five-class map
211 was reclassified to produce a final map of water and non-water for comparison with binary
212 mapping methods. All multiple-class classifications were completed using the RStoolbox
213 package including the 30-m multi-spectral Landsat bands and the 10-m national elevation dataset
214 (U.S. Geological Survey, 2015).

215 We developed optimized thresholds for mid-infrared surface reflectance, the MNDWI,
216 and the AWEInsh (non-shadow version of the AWEI) using a random forest model approach
217 (Breiman, 2001) and receiver operating characteristic (ROC) curve analysis (Fawcett, 2006). A
218 random forest model for water/non-water was built from the band or index values associated
219 with randomly selected training points (~500 each for water and non-water). We identified an
220 optimal threshold value using ROC analysis to determine the probability of membership in the
221 water class that maximized the true positive rate and minimized the false positive rate (Greiner,
222 et al., 2000). The image was then reclassified using the optimized threshold to generate a
223 water/non-water classification. To assess the utility of threshold optimization, we also produced
224 classifications using the default thresholds proposed for the MNDWI (Xu, 2006) and the
225 AWEInsh (Feyisa et al., 2014)

226 ***2.4. Optimized water/non-water threshold development***

227 We assembled ground data close in time as possible to Landsat image acquisition dates,
228 including high-resolution (0.46 - 2.5-m) imagery and field observations confirming water or non-
229 water presence on the ground from January to May for multiple years (Table 1). We identified
230 obvious water and non-water point locations from high-resolution images. Field data consisted of
231 landscape photographs of the Sacramento Valley collected as part of a separate study (Barbaree,
232 et al., 2016); fixed-wing aircraft were used to collect these photos during clear weather at
233 altitudes of 600-800m, with a final resolution of 75-150dpi. Reference datasets were
234 subsequently built from these photos by manually classifying XY coordinates as water or non-
235 water using high-resolution Google Earth imagery. We excluded reference data sources collected
236 > 10 days before or after a low-cloud cover Landsat overpass date, leaving a total of 12 reference
237 datasets corresponding with images from Landsat 5, 7 and 8 from 2006 to 2014 (Table 1). Due to

238 the lack of available February reference data, we included reference data from January to
239 represent a more comprehensive range of potential spring conditions in our study area (Table 1).

Table 1

Surface reflectance datasets and reference data sources for confirmed water and non-water locations in the Sacramento Valley of California that were incorporated in water identification threshold optimization.

DigitalGlobe data were provided by NASA's NGA Commercial Archive Data (cad4nasa.gsfc.nasa.gov) under the National Geospatial-Intelligence Agency's NextView license agreement. Field data consisted of landscape photographs of the Sacramento Valley collected as part of a separate study (Barbaree et al., 2016).

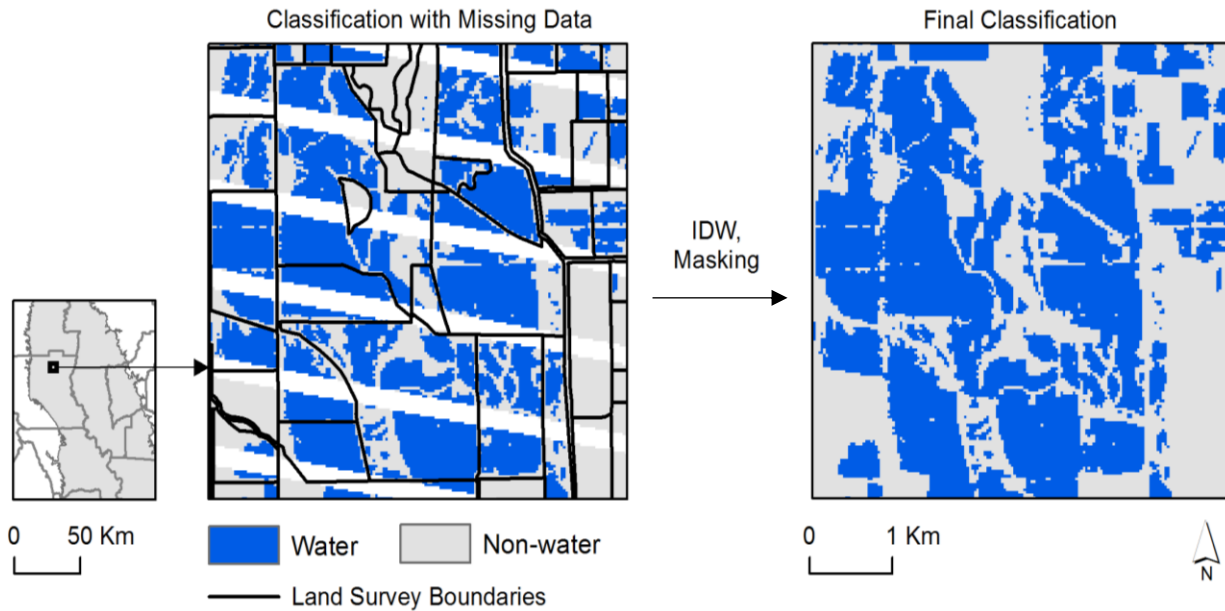
<u>Surface reflectance data</u>		<u>Reference data</u>				
Sensor	Date	Source	Date	Non-water points	Water points	Extent (km ²)
Landsat 5	2006/5/30	Quickbird	2006/5/25	110	147	349.33
Landsat 5	2008/3/18	Quickbird	2008/3/24	211	153	584.45
Landsat 5	2008/5/4	Quickbird	2008/5/4	205	255	562.73
Landsat 7	2008/5/13	Quickbird	2008/5/9	149	165	1,347.66
Landsat 7	2013/1/2	field data	2013/1/7	42	159	174.64
Landsat 7	2013/4/8	WorldView2	2013/4/10	260	329	1,436.78
Landsat 7	2013/5/10	WorldView2	2013/5/18	189	242	1,131.67
Landsat 7	2014/1/5	field data	2014/1/9	199	127	104.95
Landsat 7	2014/3/10	WorldView2	2014/3/15	760	297	2,919.3
Landsat 8	2014/1/13	field data	2014/1/9	181	120	104.95
Landsat 8	2014/3/18	WorldView2, field data	2014/3/15	766	463	3,074.06
Landsat 8	2014/4/19	field data	2014/4/11	516	188	218.63
Total				3588	2645	12,009.15

240 To identify a single threshold for separating water/non-water in spring, we incorporated
 241 mid-infrared surface reflectance values from confirmed water/non-water reference locations
 242 (Table 1). We conducted a 9-fold random forest model cross validation, withholding 3 of the 12
 243 dates from each model training set to maximize independence and rigorously assess predictive
 244 power. We identified an optimized spring water mapping threshold for our study area based on
 245 the probability of membership in the water class that maximized the true positive rate and
 246 minimized the false positive rate for the model average. To evaluate performance, we examined
 247 confusion matrices and the area under the curve (AUC) generated from cross validation of
 248 random forest model runs (Bradley, 1997).

249 *2.5. Time series image processing*

250 We applied the optimized spring mid-infrared threshold for classification of the entire
251 time series for the months of February, March, April and May from 1983-2015. We limited our
252 analysis to low-elevation, non-urban land cover unaffected by clouds and cloud shadows. Cloud
253 and shadow-free pixels were identified using the CFmask band (Zhu & Woodcock, 2012). We
254 excluded areas mapped as ‘developed’ by the most recent USDA Cropland Data Layer (USDA-
255 NASS, 2014) as well as higher elevation areas of mountainous terrain outside of the current
256 Central Valley Joint Venture planning area, which is based on topography and watersheds
257 (Central Valley Joint Venture, 2006).

258 Analyzing the full 1983 – 2015 time series necessitated the use of SLC-off Landsat 7
259 images, which are missing approximately 22% of data, even under cloud-free conditions. To
260 address this challenge, we developed a unique interpolation approach to infer water presence in
261 the areas of missing data. Much of the landscape has little elevation variation and is subject to
262 artificial flooding; therefore, we applied an inverse distance weighted (IDW) interpolation to
263 threshold classifications, using county land use survey lines collected from 1994 to 2011 as
264 boundaries (California Department of Water Resources, 2016b; Fig. 3). We also applied an IDW
265 interpolation to the CFmask to fill cloud and shadow regions in missing data areas (Zhu &
266 Woodcock, 2012). The accuracy of the IDW interpolation was assessed for a cloud-free Landsat
267 7 image acquired on March 10, 2014, using a WorldView2 image collected on the same date.



268

269 **Fig. 3.** Example of inverse distance weighted interpolation, guided by land survey boundaries (California
 270 Department of Water Resources, 2016b) applied to classifications of SLC-off Landsat 7 imagery.

271 ***2.6. Spatiotemporal analysis of shorebird habitat***

272 We analyzed long-term trends of water extent and frequency in the Sacramento Valley
 273 within the most important habitats for shorebirds: flooded agriculture and herbaceous wetlands
 274 (Central Valley Joint Venture, 2006). For each Landsat image, we calculated the proportion of
 275 water detected in the cloud-free portions of the image and estimated total water extent, in
 276 addition to water extent in each habitat type based on the most recent National Land Cover
 277 Database (Homer et al., 2015). For each two-week period in spring from 1983 - 2015, we
 278 computed mean water extent, weighting observations by the proportion of cloud-free pixels in
 279 each image. To assess long-term trends in water availability, we applied linear regression for
 280 mean water extent estimates over time within each habitat type. Within-season variability was
 281 assessed with the mean water extent and variance for each two-week period in spring; we pooled
 282 observations from all years and weighted observations by the proportion of cloud-free pixels. We

283 also calculated water frequency for each 30-m pixel by summing the total detections of water
284 presence, corrected for the total number of cloud-free instances.

285 Lastly, we explored the influence of interannual climatic variability on water extent. The
286 California Department of Water Resources reports an annual Water Year Index for the
287 Sacramento Valley based on the volume of total runoff in the river basin, which provides a
288 continuous measure of climate variation (California Department of Water Resources, 2016a).
289 This index is used to classify each water year (ending in September) as ‘Critical’, ‘Dry’, ‘Below
290 Normal’, ‘Above Normal’ or ‘Wet’. We used linear regression to assess the relationship between
291 the Water Year Index and water extent for each two-week period from 1983-2015.

292

293 **3. Results**

294 *3.1. Comparison of methods to identify water vs. non-water*

295 We compared multiple methods to map water in the study area (Table 2, Fig. S2); for the
296 thresholds, we compared the underlying random forest models and ROC analysis results (Table
297 S1) in addition to the accuracy of the final threshold classifications (Table 2). Supervised
298 classifications mapped water with high accuracy (user’s and producer’s accuracy > 98%; Table
299 2, Fig. S2). Of the threshold methods, the optimized mid-infrared reflectance threshold achieved
300 the highest overall accuracy (Table 2). Default thresholds for the water indices had lower user’s
301 accuracy for the water class than optimized thresholds developed for each index; the default
302 AWEInsh threshold was the only method to have a user’s accuracy <80%.

Table 2

Assessment of multiple methods to classify open water from a May 4, 2008 Landsat image of the Sacramento Valley (path/row 44/33) using May 4, 2008 high-resolution Quickbird imagery for reference. DigitalGlobe data were provided by NASA's NGA Commercial Archive Data (cad4nasa.gsfc.nasa.gov) under the National Geospatial-Intelligence Agency's NextView license.

Accuracy	Threshold methods ^{1,3}					Supervised methods ^{2,3}	
	Optimized mid-infrared	Default MNDWI	Optimized MNDWI	Default AWEInsh	Optimized AWEInsh	Maximum likelihood	Random forest
Overall	97.33	96.69	95.04	89.88	89.90	99.38	100.00
Water producer's	100.00	99.55	90.28	100.00	98.96	98.96	98.41
Water user's	95.76	93.67	100	79.32	80.17	98.73	98.34
Non-water producer's	93.29	94.25	100	83.45	83.96	83.96	100.00
Non-water user's	100.00	99.60	90.28	100.00	99.19	100.00	100.00

¹ Default thresholds (value = 0) were applied to the modified normalized difference water index (MNDWI) and automated water extraction index (AWEInsh, non-shadow version). Optimized mid-infrared, MNDWI and AWEInsh thresholds were identified using random forest models trained with 481 water pixels and 492 non-water pixels; receiver operating characteristic curves were used to maximize the true positive rate and minimize the false positive rate.

² Supervised classifications were trained with randomly selected water (n=490) and non-water (453 forested, 418 other green vegetation, 460 dry vegetation, and 434 urban/barren points) pixels verified from Quickbird imagery. Outputs were reclassified to water/non-water for comparison with other methods.

³ All methods were evaluated with independent reference pixels (237 water, 247 non-water).

303

304 ***3.2.Evaluation of optimized spring water/non-water mid-infrared threshold***

305 We identified a single mid-infrared threshold to map water/non-water in spring across
 306 multiple years with nine-fold cross-validation and ROC curve analysis of water/non-water
 307 random forest models (Table 3, Fig. 4). The optimal threshold for the model average that
 308 maximized the true positive rate and minimized the false positive rate occurred at a probability
 309 of 0.76 for membership in the water class (Fig. 4). This corresponded with a mid-infrared (1.5–
 310 1.7 μm) surface reflectance value of 0.069, which was determined to be the optimal threshold for
 311 separating water vs. non-water across the spring image time series in our study area. Applying

312 the spring threshold and masking steps to achieve a final classification required approximately
313 20 minutes per image in a parallelized R workflow on a computer with an i7 processor and 16GB
314 of RAM.

315 We assessed accuracy of the optimized mid-infrared threshold classification across the
316 time series using both estimates reported by associated random forest models and ROC curve
317 analysis results (Table 3, Fig. 4). Random forest models use bagging to build trees with
318 bootstrapped resampling of the training dataset, such that each tree can be tested on the out-of-
319 bag training samples not used in building that tree (Breiman, 2001). For our 9-fold cross-
320 validation of random forest models, the average out-of-bag error rate was 9.5%, with an average
321 of 11% error for the water class (Table 3). The non-water class had a lower average error rate,
322 but a higher coefficient of variation than the error rate for the water class. ROC curve analysis
323 produced accuracy estimates and an AUC for each model. The AUC measure combines the true
324 positive rate and the false positive rate for the full range of probabilities of membership in the
325 water class, where values closer to 1 represent a better classifier (Bradley, 1997). The average
326 overall threshold accuracy reported by the ROC curve analysis across models was 92% and the
327 average AUC across models was 0.94, indicating very good performance for a variety of dates
328 and environmental conditions (Table 3, Fig. 4).

Table 3

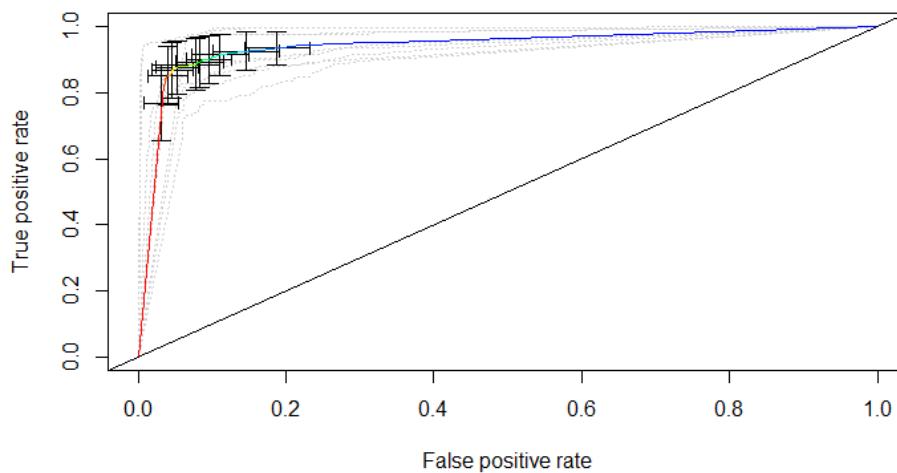
Identification of a mid-infrared surface reflectance threshold to map water and non-water the Sacramento Valley using random forest model cross-validation and receiver operating characteristic (ROC) curve analysis.

Model run ¹	Random forest error estimates			ROC curve results		Threshold accuracy		
	Water	Non-water	Average out-of-bag error	AUC	Probability threshold	Water user's accuracy	Water producer's accuracy	Overall
1	.09	.08	.09	.91	.71	.87	.88	89.13
2	.12	.08	.1	.96	.81	.88	.88	95.71
3	.11	.06	.08	.9	.76	.92	.9	86.4
4	.12	.08	.1	.97	.82	.9	.91	95.43
5	.08	.05	.07	.88	.69	.92	.9	83.97
6	.1	.09	.09	.93	.74	.89	.9	89.16
7	.13	.1	.11	.98	.75	.88	.9	97.53
8	.12	.08	.09	.94	.8	.95	.92	89.95
9	.12	.11	.12	.98	.76	.89	.89	97.53
Average	.11	.08	.1	.94	.76	.9	.9	91.65
CV	12.86	18.83	14.95	3.76	5.66	2.59	1.28	5.17

¹Each random forest model run incorporated water and non-water reference pixels from nine image dates, withholding data from three dates for accuracy assessment. ROC curve analysis identified the probability threshold for membership in the water class that maximized the true positive rate and minimized the false positive rate for each model run.

329

330



331

332 **Fig.4.** Receiver operating characteristic (ROC) curves summarizing nine-fold cross validation of water/non-water
333 random forest models used to identify a spring mid-infrared surface reflectance threshold. Dotted lines indicate ROC
334 curves for each fold of the cross validation. The colored line is the average ROC curve; cutoffs for the probability of
335 membership in the water class from 0 to 1 in increments of 0.1 are shown with error bars indicating 95% confidence
336 intervals for the true positive rate and false positive rate at each cutoff.

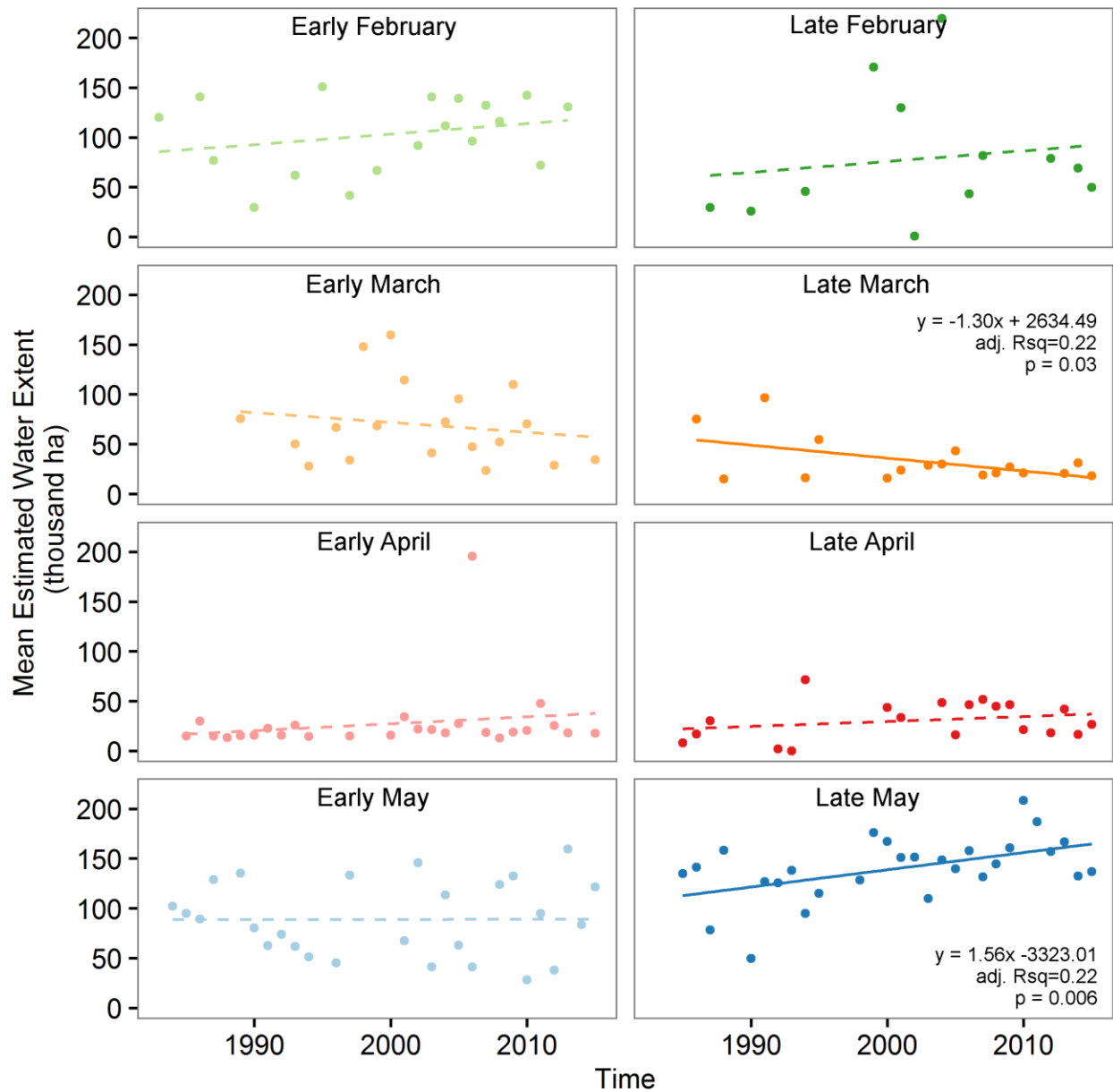
337 **3.3. Effectiveness of IDW interpolation for SLC-off Landsat 7 classifications**

338 We classified water in missing data regions with high accuracy using the spring threshold
339 and an IDW interpolation constrained by county land use survey boundaries (Fig. 3). We
340 achieved a user's accuracy of 99% (producer's = 98%) for the March 10, 2014 Landsat 7 image
341 with 213 water locations and 188 non-water locations verified using Worldview 2 imagery
342 acquired on the March 15, 2014 (Table 1). Interpolation of water/non-water and the cloud and
343 shadow mask added substantially to processing time, with up to 3.5 hours required to process
344 SLC-off Landsat 7 images (>10 times the time needed to process other images).

345 **3.4. Landsat-derived spring open water dynamics**

346 Over the study period 1983 – 2015, there was considerable variation in the estimated
347 extent of open water in the Sacramento Valley over time (Fig. 5). The average water extent in the
348 valley across the entire study period was ~75,000 ha, with a standard deviation of nearly 56,000
349 ha; both estimates were weighted by the cloud-free proportion of the study area for each
350 observation. Our highest confidence estimate of maximum extent occurred on February 19th,
351 2004 when open water was detected on nearly 215,000 ha (27% of the study area), with a cloud-
352 free view of 99% of the study area. Although the 2004 water year was ranked as having 'Below
353 Normal' precipitation (California Department of Water Resources, 2016a), above average
354 precipitation occurred that February (Daly et al., 2008). After multiple years of recent drought a

355 spring minimum extent of ~16,500 ha (~ 2% of the study area; 96% clear view) was observed on
356 March 21, 2015, slightly greater than the highest confidence minimum of ~13,000 ha (<2% of
357 the study area; 99% clear view) detected on April 11, 1988. We assessed interannual variability
358 by conducting linear regressions of the mean estimated water extent for each 2-week period from
359 1983-2015 (Fig. 5). Over the study period, water extent declined by an average of 1,300 ha per
360 year in late March (adj. $R^2=0.22$, $p=0.03$), and increased by an average of 1,560 ha per year in
361 late May (adj. $R^2 = 0.22$, $p=0.006$).

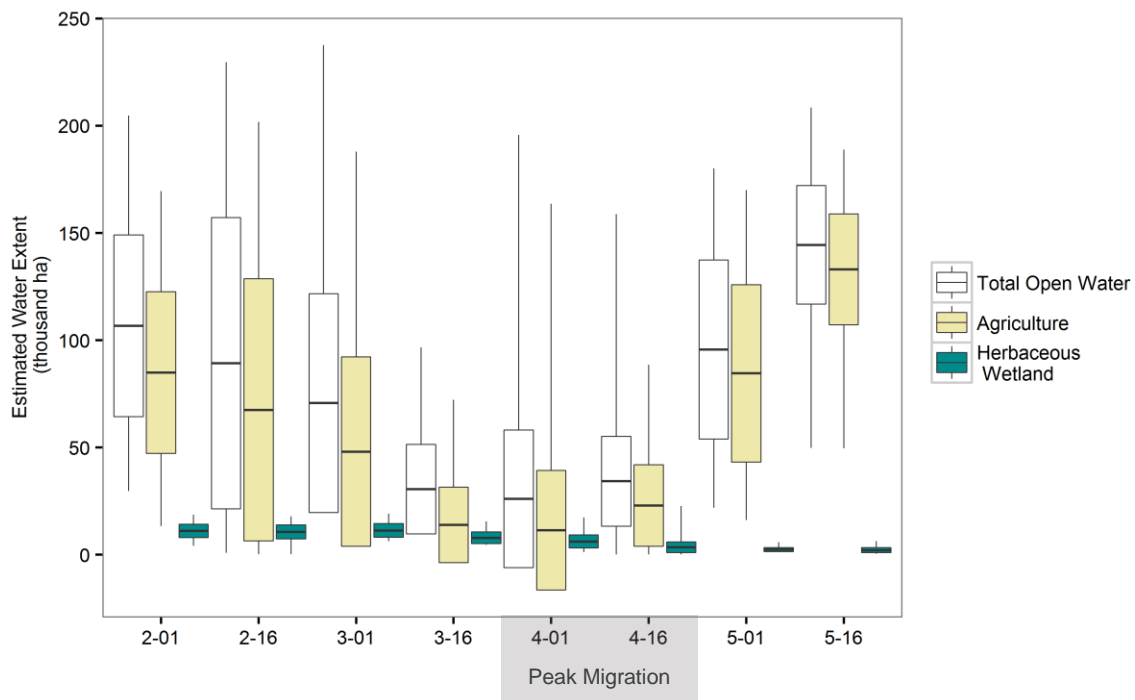


362

363 **Fig. 5.** Long-term spring water extent trends from 1983 – 2015 in the Sacramento Valley of California. Significant
 364 trends (linear regression, $p < 0.05$) are indicated by a solid line with the equation shown, while non-significant
 365 trends are indicated by dashed lines. A significant decrease in water extent in the Sacramento Valley was observed
 366 in late March, while a significant increase in water extent was observed in late May.

367 Water extent also varied substantially within the spring season, mainly due to water
 368 management on agricultural lands (Fig. 6, Table S2). The minimum flood extent consistently

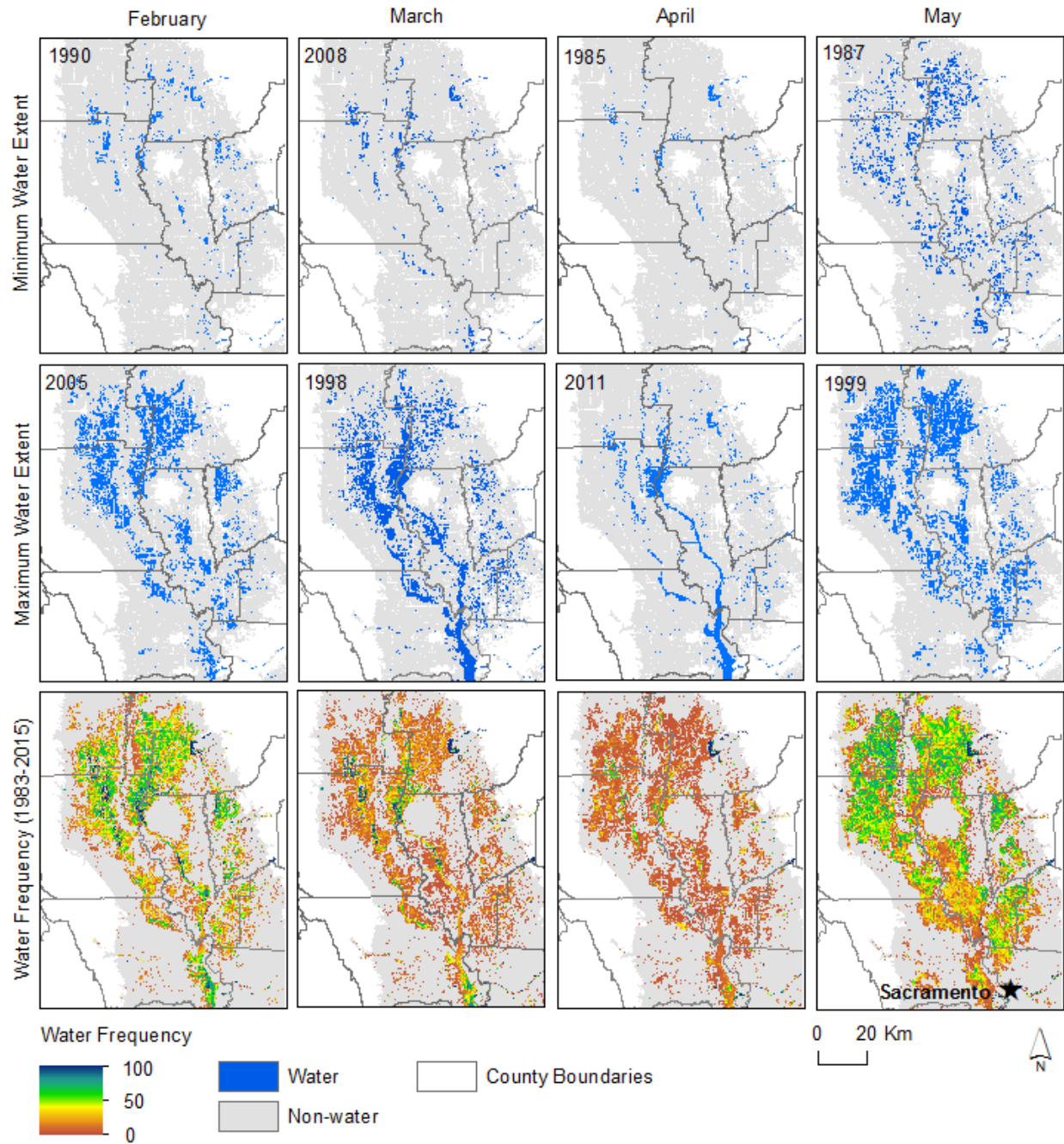
369 occurred in April (peak migration), due to a limited extent of flooded agriculture. In early April a
 370 weighted average of ~26,000 ha (~3% of the study area) +/-32,000 ha of open water was present
 371 in the Sacramento Valley (Fig. 6), whereas average extent increased by a factor of five by late
 372 May. Natural and managed wetlands were also subject to substantial within season variation;
 373 however herbaceous wetlands exhibited a different seasonal pattern from agricultural lands. Year
 374 to year, water extent within herbaceous wetlands consistently decreased beginning in March; the
 375 minimum herbaceous wetland water extent typically occurred in May (Fig. 6).



376
 377 **Fig.6.** Spring water extent and variability by two-week period in the Sacramento Valley from 1983 – 2015. Boxplots
 378 indicate the weighted mean extent and standard deviation of all open water in the valley, as well as water detected
 379 within agriculture and herbaceous wetlands for each two-week period in spring. The clear fraction of each Landsat
 380 image was used to weight observations.

381 From 1983-2015 strong within season variation in spatial water frequency patterns across
 382 the landscape was detected from our pixel-level analysis (Fig. 7, Fig. 8), revealing striking

383 differences between months. Similar to the pattern of water extent, the frequency of water
384 presence across the landscape was lowest in April. Higher water frequency was observed in
385 February and May, although the spatial patterns differed in these months. In February, high
386 water frequency areas were more spatially concentrated, and included riparian areas, reservoirs
387 and herbaceous wetlands as well as agriculture. In contrast, during May a broader swath of the
388 landscape showed moderate water frequency due to the widespread presence of active flood-
389 irrigated agriculture operations.

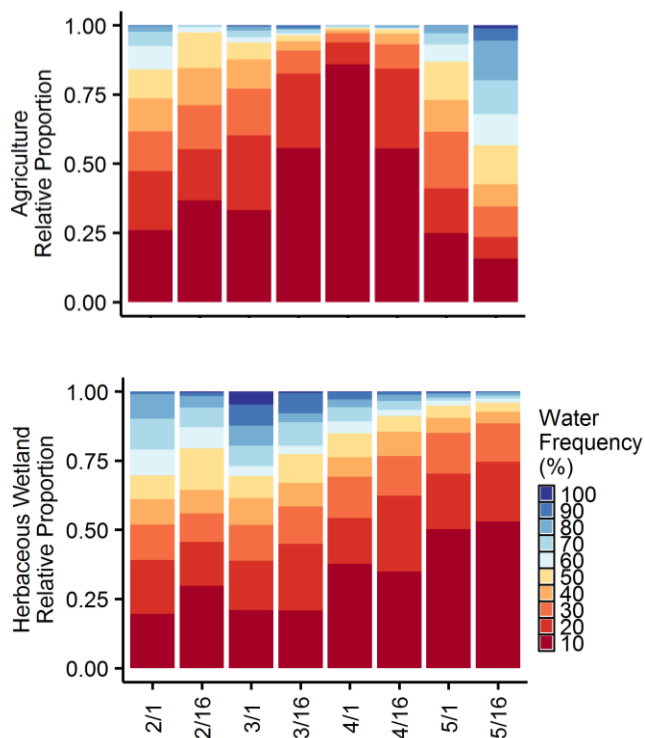


390

391 **Fig. 7.** Water extent and frequency for spring months in the Sacramento Valley from 1983-2015. Example minimum
 392 (top row) and maximum (middle row) water/non-water classifications for each month illustrate the variability of
 393 water extent in the study area; the year of each example classification is indicated at the top left of each panel. The
 394 frequency of water detection (bottom row) was calculated as the number of times water was identified in each pixel

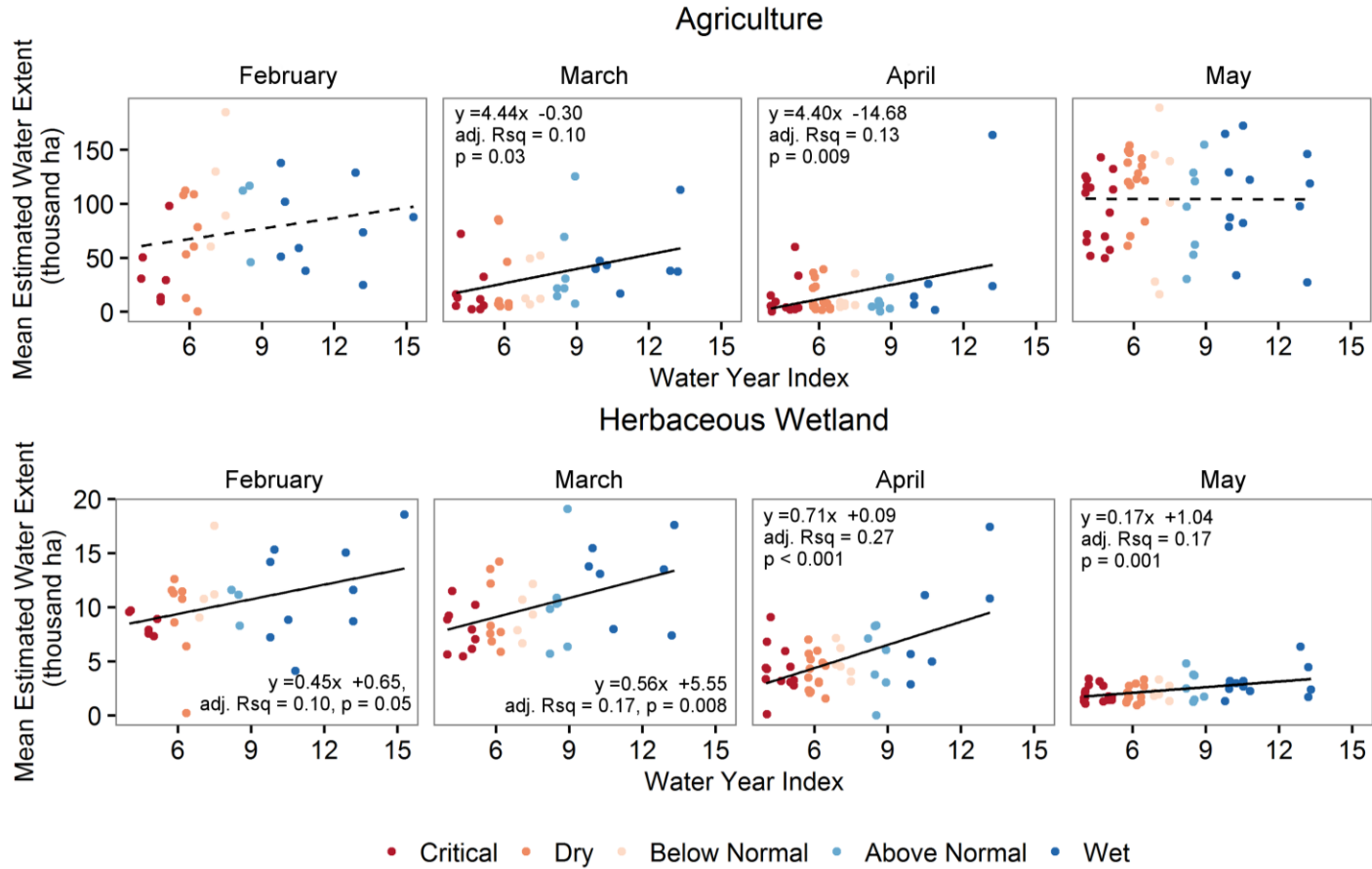
395 from a stack of all water/non-water classifications for each month from 1983-2015, corrected by the total number of
396 cloud-free instances.

397 Notable differences in the water frequency within each habitat type were observed from
398 1983-2015 (Fig. 8). During peak shorebird migration, water was detected in <10% of the cloud
399 free views for 80% of the agricultural land in the study area, while the highest water frequency in
400 agriculture was observed in May. Water was detected more reliably in herbaceous wetland
401 habitat during spring, particularly on federal and state-managed lands. Herbaceous wetland water
402 frequency was typically highest in March, becoming less reliable as the spring season
403 progressed.



404
405 **Fig. 8.** Relativized estimates of spring water frequency within flood-irrigated agriculture (A) and herbaceous
406 wetlands (B) in the Sacramento Valley from 1983-2015. Water/non-water classifications were combined for each
407 two-week spring period and the per pixel frequency of water detection was calculated, corrected by the total number
408 of cloud-free instances within each habitat type.

409 We evaluated the effect of climatic variation on water extent in each habitat type over the
410 study period using the California Department of Water Resources' Water Year Index, which
411 measures overall water availability in the Sacramento River Basin based on streamflow for each
412 water year (Fig. 9). The Water Year Index was a significant, but weak, predictor of mean water
413 extent on agricultural lands in March and April. For herbaceous wetlands, the Water Year Index
414 was a stronger predictor of water extent, and the relationship was significant for all spring
415 months. Results suggest that water presence in shorebird habitats is most sensitive to climate in
416 March and April.



417

418 **Fig. 9.** Annual water availability compared to spring water extent in flood-irrigated agriculture and herbaceous wetlands in the Sacramento Valley of California

419 from 1983 – 2015. The Water Year Index for the Sacramento River Basin scales annual water availability and designates each year as either ‘Critical’ (≤ 5.4),

420 ‘Dry’, ‘Below Normal’, ‘Above Normal’, or ‘Wet’ (≥ 9.2) (California Department of Water Resources, 2016a). Herbaceous wetland water extent was

421 significantly correlated with the Water Year Index in all spring months; while the relationship was only significant for agricultural water extent in March and

422 April (equations shown for $p < 0.05$).

423 4. Discussion

424 We measured water extent in the Sacramento Valley during spring for a time series spanning
425 more than three decades. We determined that using an optimized spring mid-infrared threshold
426 would expedite time series classification, while retaining high accuracy (Table 2, Fig. 4, Fig. S2).
427 We incorporated 63 SLC-off Landsat 7 images in the time series, using an interpolation
428 technique to accurately infer the presence of water in missing data regions. Although this data
429 processing was time intensive, it was crucial for continuity between the loss of Landsat 5 and the
430 launch of Landsat 8, and to increase the number of cloud-free observations of our study area. For
431 a long time series where processing of many images is necessary, our approach provided
432 relatively efficient and accurate estimates of water extent (Table 2). Any supervised
433 classification method would have required substantially more time to develop and refine training
434 data.

435 This work highlights the potential for threshold methods to estimate water extent over
436 time with high accuracy. A limited number of studies have explicitly compared different water
437 indices (Campos et al., 2012; Fisher et al., 2016; Ji et al., 2009; Yang et al., 2015), and fewer
438 have compared these methods against supervised classification approaches. For analysis of only
439 a few image dates, higher accuracy could likely be achieved with supervised classification
440 methods, but this becomes overly time intensive for analysis of dense images stacks. The
441 optimized threshold performed comparably to supervised classification methods that require
442 substantial user input (Table 2, Fig. 4). However, a single global water index may not work well
443 in all situations (Fisher et al., 2016; Yang et al., 2015). To take just one example, although the
444 AWEI is widely recognized as having relatively low threshold variability (Feyisa et al., 2014), its
445 success for different ecosystems was demonstrated for just five Landsat image locations. Yang *et*

446 *al.* (2015) noted that other indices sometimes outperformed AWEI in some regions, as we found
447 in this study (Table 2).

448 Only a limited number of previous studies provide methods to optimize thresholds for
449 spectral bands and water indices to local conditions (Campos et al., 2012; Fisher et al., 2016; Ji
450 et al., 2009; Sheng et al., 2016; Yang et al., 2015). If reference data are already available for
451 accuracy assessment, an optimized threshold can be developed in a matter of minutes in a
452 reproducible fashion, as we have demonstrated here with random forest models and ROC curves.
453 Other statistical optimization techniques could also be investigated such as a recent modification
454 of Otsu's method, which maximizes between-class variance, without biasing the threshold to the
455 land cover category with larger within-class variance. (Otsu, 1979; Xu, et al., 2011).

456 Identifying a global water identification threshold is an attractive concept; however, we
457 suspect that optimized thresholds will be more effective at local and regional scales, or within
458 ecotypes. Fisher *et al.* (2016) developed a single threshold for a large area in Eastern Australia;
459 however, this required hundreds of thousands of training points, which is not a practical
460 undertaking in most cases. Furthermore, the authors did not explicitly test the accuracy of their
461 single threshold outside of the training source areas. It makes perfect sense to use thresholds
462 from the literature as a starting point for analysis; however, if reference data are available, we
463 propose that researchers should tailor thresholds to their study area and period.

464 Tracking water trends over 32 years revealed important information about shorebird
465 habitat dynamics in the Sacramento Valley. Our finding that the minimum water extent occurs
466 during the peak of spring shorebird migration (Fig. 6, Fig. 7) corroborates other studies
467 (Barbaree et al., 2015; Central Valley Joint Venture, 2006) and stresses the need for conservation
468 and management actions focused on this particular window of time. The decline in March water

469 extent that we quantified gives further credence to concern that the Sacramento Valley may not
470 provide sufficient habitat for migrating shorebirds, particularly during drought conditions
471 (Central Valley Joint Venture 2006). Water allocation decisions and the timing of flooding and
472 drawdown of wetlands and agricultural fields have a strong influence on habitat and food
473 availability; these factors therefore affect shorebird abundance and residence time in the valley.
474 Non-linear spring water fluctuations (Fig. 5-9, Table S2) reflect practices in flood-irrigated rice
475 fields, contrasting from fall migration in recent years where water extent consistently increased
476 from September through December (Reiter et al., 2015). Managed wetlands in the Sacramento
477 Valley provide an important source of stable habitat for shorebirds; when agricultural water
478 reaches its spring minimum extent, managed wetlands provide a comparable amount of core
479 open water habitat. Consistent late winter and spring water habitats, such as that provided by the
480 National Wildlife Refuge System and State Wildlife Management Areas, are especially crucial in
481 years when agricultural flooding is delayed, or reduced due to water allocation restrictions.

482 Our findings have implications for wetland management under a changing climate. Water
483 extent within both herbaceous wetlands and flood-irrigated agriculture was significantly
484 correlated with the California Department of Water Resources' Water Year Index. While
485 agricultural water extent was less sensitive to fluctuations in water availability, it will be affected
486 by climate change and emerging water policy. Precipitation in the Sierra Nevada is projected to
487 decrease, particularly the amount and duration of the winter snowpack (Cayan et al., 2008),
488 which is the main source of surface water in warmer, drier spring and summer months. In 2015,
489 the state water project delivered just one-fifth of the water requested by users and a zero
490 allocation was issued by the federal water project ("Watering California's Farms," 2015).
491 Although farmers have historically pumped groundwater to supplement limited surface water

492 supplies, particularly in years with low precipitation, legislation to regulate groundwater
493 pumping recently passed in California (Sustainable Groundwater Management Act, 2014).
494 Continued water deficits have heightened scrutiny of all forms of water use, and agriculture has
495 been a popular target; rice production in 2014 was down 25% compared to the previous year, and
496 there is increasing pressure for growers to reduce water use through drip irrigation (“Watering
497 California’s Farms,” 2015). A move away from flood irrigation over large areas could provide
498 substantial water savings, however it would also dramatically change shorebird habitat in the
499 Sacramento Valley and other stopovers where extensive flood irrigation is currently practiced.
500 Such changes in water management could result in reduced yields, shifts in the types of crops
501 cultivated, and add strain on the livelihoods of the farmers that produce food for domestic and
502 foreign consumers.

503 Our analysis faced some limitations. The Sacramento Valley was frequently affected by
504 fog or cloud cover, particularly during El Niño conditions, and although Landsat’s overpass
505 interval increased with the launch of Landsat 7, a substantial portion of available data comprised
506 SLC-off imagery (Fig. 2). In addition to Landsat data limitations, high-resolution imagery and
507 other reference datasets were not available for earlier years. As for observation frequency, it is
508 possible that some agricultural fields may transition from flooded to drained within four days
509 (unpublished results), in contrast to Landsat’s current 8-day overpass interval. This is unique to
510 agricultural fields, as opposed to wetlands which draw down more gradually, and can affect
511 collection of data to validate water presence and other characteristics of interest (Turpie et al.,
512 2015). Water features may also be subject to confusion with topography and urban development;
513 fortunately, our study area included low-elevation water features in rural areas. Estimates of
514 water extent likely underestimated habitat availability, for example in moist soil at the field

515 edges and in areas obscured by dense emergent vegetation. Saturated area could be estimated
516 from our water/non-water classification products by calculating the total length of water
517 perimeters detected in the landscape.

518 Multiple stakeholders in California are recognizing the value of Landsat-derived water
519 extent maps for management decisions. Our technique could expedite near real time mapping
520 and monitoring efforts to inform policymakers in California, and in other regions experiencing
521 water stress. Given access to sufficient training data, our approach could be modified and
522 extended in order to meet the needs of research questions in other seasons, or other regions. The
523 increased availability of high-resolution reference images such as the National Agricultural
524 Imagery Program (U.S. Department of Agriculture Farm Services Agency, 2016) and Google
525 Earth offer promising data sources that can be harnessed for threshold optimization in future
526 studies of water dynamics.

527

528 **5. Conclusions**

529 In this study, we mapped open water from a 32-year Landsat time series using an
530 optimized mid-infrared reflectance threshold. Thresholds that were optimized using random
531 forest models and ROC curve analysis produced water classifications with higher user's accuracy
532 than classifications using thresholds from the literature. Despite the irregularity of data
533 availability and cloud cover, we were able to gather sufficient data from Landsat's extensive
534 record to accomplish an analysis of long-term water extent trends within important habitats for
535 migratory shorebirds. Interpolated classifications of Landsat 7 imagery provided a valuable data
536 source for tracking water dynamics when other cloud-free images were not available. Our

537 analysis revealed strong effects of climate and land management on the extent of water in
538 Sacramento Valley wetlands and flood-irrigated agriculture. Water extent has been most limited
539 at the peak of migration, when shorebirds urgently need flooded habitat for resting and foraging.
540 Quantified reductions in March water extent also indicate that the amount of habitat leading into
541 peak migration is dwindling. This study demonstrates the value for water and habitat
542 management that can be drawn from analyzing an extended remotely-sensed time series.
543 Additionally, adaptation of the reproducible threshold optimization demonstrated here can yield
544 efficient high accuracy classifications of water in other regions.

545

546 **Acknowledgements**

547 Schaffer-Smith's work was supported by a NASA Earth and Space Science Fellowship
548 (NNX13AQ15H) and an NSF DDRI Award (1459226). DigitalGlobe data were provided by
549 NASA's NGA Commercial Archive Data (cad4nasa.gsfc.nasa.gov) under the National
550 Geospatial-Intelligence Agency's NextView license agreement. We thank Kemen G. Austin,
551 Brenna R. Forester, Mariano González-Roglich, and Amanda M. Schwantes for offering
552 valuable feedback. Two anonymous reviewers also provided comments that greatly improved
553 this work.

554

555 **References**

556 Alsdorf, D. E., Rodríguez, E., & Lettenmaier, D. P. (2007). Measuring surface water from space.
557 *Reviews of Geophysics*, 45(2). <https://doi.org/10.1029/2006RG000197>

558 Baker, C., Lawrence, R., Montagne, C., & Patten, D. (2006). Mapping wetlands and riparian
559 areas using Landsat ETM+ imagery and decision-tree-based models. *Wetlands*, 26(2),
560 465–474. [https://doi.org/10.1672/0277-5212\(2006\)26\[465:MWARAU\]2.0.CO;2](https://doi.org/10.1672/0277-5212(2006)26[465:MWARAU]2.0.CO;2)

561 Barbaree, B. A., Reiter, M. E., Hickey, C. M., & Page, G. W. (2015). Day and Night Habitat
562 Associations of Wintering Dunlin (*Calidris alpina*) within an Agriculture-Wetland
563 Mosaic. *Waterbirds*, 38(1), 40–46. <https://doi.org/10.1675/063.038.0106>

564 Barbaree, B. A., Reiter, M. E., Hickey, C. M., & Page, G. W. (2016). Molt migration and
565 migratory connectivity of the long-billed dowitcher: Dowitchers in the Klamath Basin
566 and Central Valley. *The Journal of Wildlife Management*, 80(2), 256–265.
567 <https://doi.org/10.1002/jwmg.1006>

568 Batzer, D. P. (2013). The Seemingly Intractable Ecological Responses of Invertebrates in North
569 American Wetlands: A Review. *Wetlands*, 33(1), 1–15. [https://doi.org/10.1007/s13157-](https://doi.org/10.1007/s13157-012-0360-2)
570 [012-0360-2](https://doi.org/10.1007/s13157-012-0360-2)

571 Bontemps, S., Defourny, P., Bogaert, E. V., Arino, O., Kalogirou, V., & Perez, J. R. (2011).
572 *GLOBCOVER 2009--Products description and validation report* (p. 53). UCLouvain &
573 ESA Team. Retrieved from
574 http://due.esrin.esa.int/files/GLOBCOVER2009_Validation_Report_2.2.pdf

575 Bradley, A. P. (1997). The use of the area under the ROC curve in the evaluation of machine
576 learning algorithms. *Pattern Recognition*, 30(7), 1145–1159.
577 [https://doi.org/10.1016/S0031-3203\(96\)00142-2](https://doi.org/10.1016/S0031-3203(96)00142-2)

578 Breiman, L. (2001). Random forests. *Machine Learning*, 45(1), 5–32.
579 <https://doi.org/10.1023/A:1010933404324>

580 Brown, S., Hickey, C. M., Harrington, B., & Gill, R. (2001). U.S. Shorebird Conservation Plan,
581 second edition. Manomet Center for Conservation Sciences. Retrieved from
582 <http://www.shorebirdplan.org/>

583 California Department of Water Resources. (2016a). Chronological Reconstructed Sacramento
584 and San Joaquin Valley Water Year Hydrologic Classification Indices. California Data
585 Exchange Center. Retrieved from <http://cdec.water.ca.gov/cgi-progs/iodir/WSIHIST>

586 California Department of Water Resources. (2016b). *Land Use Survey: Amador, Butte,*
587 *Calaveras, Colusa , El Dorado, Glenn, Nevada, Placer, Sacramento, San Joaquin,*
588 *Stanislaus, Sutter, Tehama, Tuolumne, Yolo, Yuba Counties.* Retrieved from
589 <http://www.water.ca.gov/landwateruse/lusrvymain.cfm>

590 Campos, J. C., Sillero, N., & Brito, J. C. (2012). Normalized difference water indexes have
591 dissimilar performances in detecting seasonal and permanent water in the Sahara–Sahel
592 transition zone. *Journal of Hydrology*, 464–465, 438–446.
593 <https://doi.org/10.1016/j.jhydrol.2012.07.042>

594 Cayan, D. R. (1996). Interannual Climate Variability and Snowpack in the Western United
595 States. *Journal of Climate*, 9(5), 928–948. [https://doi.org/10.1175/1520-](https://doi.org/10.1175/1520-0442(1996)009<0928:ICVASI>2.0.CO;2)
596 [0442\(1996\)009<0928:ICVASI>2.0.CO;2](https://doi.org/10.1175/1520-0442(1996)009<0928:ICVASI>2.0.CO;2)

597 Cayan, D. R., Maurer, E. P., Dettinger, M. D., Tyree, M., & Hayhoe, K. (2008). Climate change
598 scenarios for the California region. *Climatic Change*, 87(S1), 21–42.
599 <https://doi.org/10.1007/s10584-007-9377-6>

600 Central Valley Joint Venture. (2006). Central Valley Joint Venture Implementation Plan -
601 Conserving Bird Habitat. U.S. Fish and Wildlife Service, Sacramento, CA. Retrieved
602 from http://www.centralvalleyjointventure.org/assets/pdf/CVJV_fnl.pdf

603 Chuvieco, E. (2016). *Fundamentals of satellite remote sensing: an environmental approach*.
604 Retrieved from <http://marc.crcnetbase.com/isbn/9781498728072>

605 Davidson, N. C. (2014). How much wetland has the world lost? Long-term and recent trends in
606 global wetland area. *Marine and Freshwater Research*, 65(10), 934.
607 <https://doi.org/10.1071/MF14173>

608 Dudgeon, D., Arthington, A. H., Gessner, M. O., Kawabata, Z.-I., Knowler, D. J., Lévêque, C.,
609 Naiman, R.J., Prieur-Richard, A.-H., Soto, D., Stiassny, M. L. J., & Sullivan, C. A.
610 (2005). Freshwater biodiversity: importance, threats, status and conservation challenges.
611 *Biological Reviews*, 81(2), 163. <https://doi.org/10.1017/S1464793105006950>

612 Elphick, C. S. (2000). Functional equivalency between rice fields and seminatural wetland
613 habitats. *Conservation Biology*, 14(1), 181–191. <https://doi.org/10.1046/j.1523-1739.2000.98314.x>

614

615 Elphick, C. S. (2008). Landscape Effects on Waterbird Densities in California Rice Fields:
616 Taxonomic Differences, Scale-Dependence, and Conservation Implications. *Waterbirds*,
617 31(1), 62–69. [https://doi.org/10.1675/1524-4695\(2008\)31\[62:LEOWDI\]2.0.CO;2](https://doi.org/10.1675/1524-4695(2008)31[62:LEOWDI]2.0.CO;2)

618 Elphick, C. S. (2010). Why Study Birds in Rice Fields? *Waterbirds*, 33(sp1), 1–7.
619 <https://doi.org/10.1675/063.033.s101>

620 ESRI. (2014). *ArcGIS Desktop, version 10.3*. Redlands, CA: Environmental Systems Research
621 Institute.

622 Farmer, A. H., & Parent, A. H. (1997). Effects of the landscape on shorebird movements at
623 spring migration stopovers. *The Condor*, 99, 698–707.

624 Fawcett, T. (2006). An introduction to ROC analysis. *Pattern Recognition Letters*, 27(8), 861–
625 874. <https://doi.org/10.1016/j.patrec.2005.10.010>

626 Feldl, N., & Roe, G. H. (2011). Climate Variability and the Shape of Daily Precipitation: A Case
627 Study of ENSO and the American West. *Journal of Climate*, 24(10), 2483–2499.
628 <https://doi.org/10.1175/2010JCLI3555.1>

629 Feng, L., Han, X., Hu, C., & Chen, X. (2016). Four decades of wetland changes of the largest
630 freshwater lake in China: Possible linkage to the Three Gorges Dam? *Remote Sensing of*
631 *Environment*, 176, 43–55. <https://doi.org/10.1016/j.rse.2016.01.011>

632 Feyisa, G. L., Meilby, H., Fensholt, R., & Proud, S. R. (2014). Automated Water Extraction
633 Index: A new technique for surface water mapping using Landsat imagery. *Remote*
634 *Sensing of Environment*, 140, 23–35. <https://doi.org/10.1016/j.rse.2013.08.029>

635 Fisher, A., Flood, N., & Danaher, T. (2016). Comparing Landsat water index methods for
636 automated water classification in eastern Australia. *Remote Sensing of Environment*, 175,
637 167–182. <https://doi.org/10.1016/j.rse.2015.12.055>

638 Fluet-Chouinard, E., Lehner, B., Rebelo, L.-M., Papa, F., & Hamilton, S. K. (2015).
639 Development of a global inundation map at high spatial resolution from topographic
640 downscaling of coarse-scale remote sensing data. *Remote Sensing of Environment*, 158,
641 348–361. <https://doi.org/10.1016/j.rse.2014.10.015>

642 Frayer, W. E., Peters, D. D., & Pywell, H. R. (1989). Wetlands of the California Central Valley:
643 Status and trends, 1939 to mid-1980's. 28pp. U.S. Fish and Wildlife Service, Portland,
644 Oregon.

645 Friedl, M. A., & Brodley, C. E. (1997). Decision tree classification of land cover from remotely
646 sensed data. *Remote Sensing of Environment*, 61(3), 399–409.
647 [https://doi.org/10.1016/S0034-4257\(97\)00049-7](https://doi.org/10.1016/S0034-4257(97)00049-7)

648 Galbraith, H., Jones, R., Park, R., Clough, J., Herrod-Julius, S., Harrington, B., & Page, G.
649 (2002). Global Climate Change and Sea Level Rise: Potential Losses of Intertidal Habitat
650 for Shorebirds. *Waterbirds*, 25(2), 173–183. [https://doi.org/10.1675/1524-](https://doi.org/10.1675/1524-4695(2002)025[0173:GCCASL]2.0.CO;2)
651 [4695\(2002\)025\[0173:GCCASL\]2.0.CO;2](https://doi.org/10.1675/1524-4695(2002)025[0173:GCCASL]2.0.CO;2)

652 Grantham, T. E., & Viers, J. H. (2014). 100 years of California’s water rights system: patterns,
653 trends and uncertainty. *Environmental Research Letters*, 9(8), 84012.
654 <https://doi.org/10.1088/1748-9326/9/8/084012>

655 Greenberg, J. A. (2014). spatial.tools: R functions for working with spatial data. R package
656 version 1.4.8. Retrieved from <https://CRAN.R-project.org/package=spatial.tools>

657 Greiner, M., Pfeiffer, D., & Smith, R. D. (2000). Principles and practical application of the
658 receiver-operating characteristic analysis for diagnostic tests. *Preventive Veterinary*
659 *Medicine*, 45(1–2), 23–41. [https://doi.org/10.1016/S0167-5877\(00\)00115-X](https://doi.org/10.1016/S0167-5877(00)00115-X)

660 Hurrell, J. W., & Loon, H. (1997). Decadal Variations in Climate Associated with the North
661 Atlantic Oscillation. In H. F. Diaz, M. Beniston, & R. S. Bradley (Eds.), *Climatic Change*
662 *at High Elevation Sites* (pp. 69–94). Dordrecht: Springer Netherlands. Retrieved from
663 http://link.springer.com/10.1007/978-94-015-8905-5_4

664 Jenkins, M. W., Lund, J. R., Howitt, R. E., Draper, A. J., Msangi, S. M., Tanaka, S. K., Ritzema,
665 R. S., & Marques, G. F. (2004). Optimization of California’s Water Supply System:
666 Results and Insights. *Journal of Water Resources Planning and Management*, 130(4),
667 271–280. [https://doi.org/10.1061/\(ASCE\)0733-9496\(2004\)130:4\(271\)](https://doi.org/10.1061/(ASCE)0733-9496(2004)130:4(271))

668 Ji, L., Zhang, L., & Wylie, B. (2009). Analysis of Dynamic Thresholds for the Normalized
669 Difference Water Index. *Photogrammetric Engineering & Remote Sensing*, 75(11),
670 1307–1317. <https://doi.org/10.14358/PERS.75.11.1307>

671 Lee, Z., Carder, K. L., Mobley, C. D., Steward, R. G., & Patch, J. S. (1999). Hyperspectral
672 Remote Sensing for Shallow Waters. 2. Deriving Bottom Depths and Water Properties by
673 Optimization. *Applied Optics*, 38(18), 3831. <https://doi.org/10.1364/AO.38.003831>

674 Lehner, B., & Döll, P. (2004). Development and validation of a global database of lakes,
675 reservoirs and wetlands. *Journal of Hydrology*, 296(1–4), 1–22.
676 <https://doi.org/10.1016/j.jhydrol.2004.03.028>

677 Leutner, B., & Horning, N. (2016). *RStoolbox: Tools for Remote Sensing Data Analysis*. R
678 *package version 0.1.4*. Retrieved from <https://CRAN.R-project.org/package=RStoolbox>

679 Liaw, A., & Wiener, M. (2002). Classification and regression by randomForest. *R News*, 2(3),
680 18–22.

681 Lyzenga, D. R., Malinas, N. P., & Tanis, F. J. (2006). Multispectral bathymetry using a simple
682 physically based algorithm. *IEEE Transactions on Geoscience and Remote Sensing*,
683 44(8), 2251–2259. <https://doi.org/10.1109/TGRS.2006.872909>

684 Maggioni, E. (2015). Water demand management in times of drought: What matters for water
685 conservation. *Water Resources Research*, 51(1), 125–139.
686 <https://doi.org/10.1002/2014WR016301>

687 Masek, J.G, Vermote, E.F., Saleous, N., Wolfe, R., Hall, F.G., Huemmrich, K.F., Gao, F.,
688 Kutler, J., & Lim, T.K. (2013). LEDAPS Calibration, Reflectance, Atmospheric
689 Correction Preprocessing Code, Version 2. <https://doi.org/10.3334/ORNLDAAAC/1146>

690 Mather, P. M. (1985). A computationally-efficient maximum-likelihood classifier employing
691 prior probabilities for remotely-sensed data. *International Journal of Remote Sensing*,
692 6(2), 369–376. <https://doi.org/10.1080/01431168508948456>

693 McFeeters, S. K. (1996). The use of the Normalized Difference Water Index (NDWI) in the
694 delineation of open water features. *International Journal of Remote Sensing*, *17*(7),
695 1425–1432. <https://doi.org/10.1080/01431169608948714>

696 Morrison, R. I. G., McCaffery, B. J., Gill, R. E., Skagen, S. K., Jones, S. L., Page, G. W., Gratto-
697 Trevor, C. L., & Andres, B. A. (2006). Population estimates of North American
698 shorebirds, 2006. *Wader Study Group Bulletin*, *11*, 67–85.

699 Mueller, N., Lewis, A., Roberts, D., Ring, S., Melrose, R., Sixsmith, J., Lymburner, L.,
700 McIntyre, A., Tan, P., Curnow, S., & Ip, A. (2016). Water observations from space:
701 Mapping surface water from 25 years of Landsat imagery across Australia. *Remote*
702 *Sensing of Environment*, *174*, 341–352. <https://doi.org/10.1016/j.rse.2015.11.003>

703 NOAA National Centers for Environmental Information. (2016). NOAA’s Gridded Climate
704 Divisional Dataset (CLIMDIV). [California Division 02]. Retrieved from
705 <https://www.ncdc.noaa.gov/>

706 Otsu, N. (1979). A threshold selection method from gray-level histograms. *Automatica*, *11*(285–
707 296), 23–27.

708 Ozesmi, S. L., & Bauer, M. E. (2002). Satellite remote sensing of wetlands. *Wetlands Ecology*
709 *and Management*, *10*(5), 381–402.

710 Papa, F., Prigent, C., Aires, F., Jimenez, C., Rossow, W. B., & Matthews, E. (2010). Interannual
711 variability of surface water extent at the global scale, 1993–2004. *Journal of Geophysical*
712 *Research*, *115*(D12), 1–17. <https://doi.org/10.1029/2009JD012674>

713 Perpignan Lamigueiro, O., & Hijmans, R. (2016). *rasterVis*. R package version 0.40. Retrieved
714 from <http://oscarperpignan.github.io/rastervis/>

715 Pimentel, D., Berger, B., Filiberto, D., Newton, M., Wolfe, B., Karabinakis, E., Clark, S., Poon,
716 E., Abbett, E., & Nandagopal, S. (2004). Water Resources: Agricultural and
717 Environmental Issues. *BioScience*, 54(10), 909. [https://doi.org/10.1641/0006-](https://doi.org/10.1641/0006-3568(2004)054[0909:WRAAEI]2.0.CO;2)
718 [3568\(2004\)054\[0909:WRAAEI\]2.0.CO;2](https://doi.org/10.1641/0006-3568(2004)054[0909:WRAAEI]2.0.CO;2)

719 Prigent, C., Papa, F., Aires, F., Rossow, W. B., & Matthews, E. (2007). Global inundation
720 dynamics inferred from multiple satellite observations, 1993–2000. *Journal of*
721 *Geophysical Research*, 112(D12). <https://doi.org/10.1029/2006JD007847>

722 Reiter, M. E., Elliott, N., Veloz, S., Jongsomjit, D., Hickey, C. M., Merrifield, M., & Reynolds,
723 M. D. (2015). Spatio-Temporal Patterns of Open Surface Water in the Central Valley of
724 California 2000-2011: Drought, Land Cover, and Waterbirds. *JAWRA Journal of the*
725 *American Water Resources Association*, 51(6), 1722–1738. [https://doi.org/10.1111/1752-](https://doi.org/10.1111/1752-1688.12353)
726 [1688.12353](https://doi.org/10.1111/1752-1688.12353)

727 Reiter, M. E., & Liu, L. (2011). The Distribution of Early-Winter Flooding in the Central Valley
728 of California: 2000 – 2010. Report to The California Landscape Conservation
729 Cooperative. PRBO Conservation Science, Petaluma, California.

730 Sheng, Y., Song, C., Wang, J., Lyons, E. A., Knox, B. R., Cox, J. S., & Gao, F. (2016).
731 Representative lake water extent mapping at continental scales using multi-temporal
732 Landsat-8 imagery. *Remote Sensing of Environment*, 185, 129–141.
733 <https://doi.org/10.1016/j.rse.2015.12.041>

734 Shuford, W. D., Page, G. W., & Kjelson, J. E. (1998). Patterns and Dynamics of Shorebird Use
735 of California's Central Valley. *The Condor*, 100(2), 227–244.
736 <https://doi.org/10.2307/1370264>

737 Sing, T., Sander, O., Beerenwinkel, N., & Lengauer, T. (2005). ROCR: visualizing classifier
738 performance in R. *Bioinformatics*, *21*(20), 3940–3941.
739 <https://doi.org/10.1093/bioinformatics/bti623>

740 Spell, R., Lewis, A., Kempka, R., & Ried, F. A. (1995). Evaluation of winter flooding of
741 ricelands in the Central Valley of California using satellite imagery. In K. L. Campbell
742 (Ed.), *Versatility of wetlands in the agricultural landscape* (Vol. 1, pp. 357–366). St.
743 Joseph, MI: American Society of Agricultural Engineers.

744 Strum, K. M., Reiter, M. E., Hartman, C. A., Iglecia, M. N., Kelsey, T. R., & Hickey, C. M.
745 (2013). Winter management of California’s rice fields to maximize waterbird habitat and
746 minimize water use. *Agriculture, Ecosystems & Environment*, *179*, 116–124.
747 <https://doi.org/10.1016/j.agee.2013.08.003>

748 Sustainable Groundwater Management Act, Pub. L. No. AB 1739 (Dickinson), SB 1168
749 (Pavley), and SB 1319 (Pavley) (2014).

750 Tulbure, M. G., & Broich, M. (2013). Spatiotemporal dynamic of surface water bodies using
751 Landsat time-series data from 1999 to 2011. *ISPRS Journal of Photogrammetry and*
752 *Remote Sensing*, *79*, 44–52. <https://doi.org/10.1016/j.isprsjprs.2013.01.010>

753 Tulbure, M. G., Broich, M., Stehman, S. V., & Kommareddy, A. (2016). Surface water extent
754 dynamics from three decades of seasonally continuous Landsat time series at
755 subcontinental scale in a semi-arid region. *Remote Sensing of Environment*, *178*, 142–
756 157. <https://doi.org/10.1016/j.rse.2016.02.034>

757 Turpie, K. R., Allen, D. W., Ackelson, S., Bell, T., Dierssen, H., Cavanaugh, K., Fisher, J. B.,
758 Goodman, J., Guild, L., Hochberg, E., Klemas, V. V., Lavender, S., Lee, C., Muller-
759 Karger, F., Ortiz, J., Palacios, S., Thompson, D. R., & Zimmerman, R. (2015). New Need

760 to Understand Changing Coastal and Inland Aquatic Ecosystem Services.
761 <https://doi.org/10.13140/RG.2.1.5162.6007>

762 U.S. Department of Agriculture Farm Services Agency. (2016). National Agriculture Imagery
763 Program. Retrieved from [http:// datagateway.nrcs.usda.gov](http://datagateway.nrcs.usda.gov)

764 U.S. Geological Survey. (2015). 10m National Elevation Dataset. Retrieved from
765 <http://ned.usgs.gov/>

766 USDA-NASS. (2014). Agricultural statistics data base. USDA-NASS, Washington DC.
767 Retrieved from www.nass.usda.gov

768 Van Loon, A. F., Gleeson, T., Clark, J., Van Dijk, A. I. J. M., Stahl, K., Hannaford, J., Di
769 Baldassarre, G., Teuling, A. J., Tallaksen, L. M., Uijlenhoet, R., Hannah, D. M.,
770 Sheffield, J., Svoboda, M., Verbeiren, B., Wagener, T., Rangescroft, S., Wanders, N., &
771 Van Lanen, H. A. J. (2016). Drought in the Anthropocene. *Nature Geoscience*, 9(2), 89–
772 91. <https://doi.org/10.1038/ngeo2646>

773 VanDerWal, J., Falconi, L., Januchowski, S., Shoo, L., & Storlie, C. (2014). *SDMTools: Species*
774 *Distribution Modelling Tools: Tools for processing data associated with species*
775 *distribution modelling exercises. R package version 1.1-221*. Retrieved from
776 <https://CRAN.R-project.org/package=SDMTools>

777 Vermote, E., Justice, C., Claverie, M., & Franch, B. (2016). Preliminary analysis of the
778 performance of the Landsat 8/OLI land surface reflectance product. *Remote Sensing of*
779 *Environment*, 185, 46–56. <https://doi.org/10.1016/j.rse.2016.04.008>

780 Verpoorter, C., Kutser, T., Seekell, D. A., & Tranvik, L. J. (2014). A global inventory of lakes
781 based on high-resolution satellite imagery. *Geophysical Research Letters*, 41(18), 6396–
782 6402. <https://doi.org/10.1002/2014GL060641>

783 Watering California's Farms. (2015, April 4). *The New York Times*.

784 Wegmann, M., Leutner, B., & Dech, S. (Eds.). (2015). *Remote sensing and GIS for ecologists*.
785 Exeter: Pelagic Publishing.

786 Werner, B. A., Johnson, W. C., & Guntenspergen, G. R. (2013). Evidence for 20th century
787 climate warming and wetland drying in the North American Prairie Pothole Region.
788 *Ecology and Evolution*, 3471–3482. <https://doi.org/10.1002/ece3.731>

789 Western Hemisphere Shorebird Reserve Network. (2009). Western Hemisphere Shorebird
790 Reserve Network List of Sites. Retrieved November 3, 2016, from
791 <http://www.whsrn.org/sites/list-sites>

792 Wickham, H. (2007). Reshaping Data with the **reshape** Package. *Journal of Statistical Software*,
793 21(12). <https://doi.org/10.18637/jss.v021.i12>

794 Wickham, H. (2009). *Ggplot2: elegant graphics for data analysis*. New York: Springer.

795 Wickham, H., & Francois, R. (2015). *dplyr: A Grammar of Data Manipulation*. R package
796 version 0.4.3. Retrieved from <https://CRAN.R-project.org/package=dplyr>

797 Xu, H. (2006). Modification of normalised difference water index (NDWI) to enhance open
798 water features in remotely sensed imagery. *International Journal of Remote Sensing*,
799 27(14), 3025–3033. <https://doi.org/10.1080/01431160600589179>

800 Xu, X., Xu, S., Jin, L., & Song, E. (2011). Characteristic analysis of Otsu threshold and its
801 applications. *Pattern Recognition Letters*, 32(7), 956–961.
802 <https://doi.org/10.1016/j.patrec.2011.01.021>

803 Yang, Y., Liu, Y., Zhou, M., Zhang, S., Zhan, W., Sun, C., & Duan, Y. (2015). Landsat 8 OLI
804 image based terrestrial water extraction from heterogeneous backgrounds using a

805 reflectance homogenization approach. *Remote Sensing of Environment*, 171, 14–32.

806 <https://doi.org/10.1016/j.rse.2015.10.005>

807 Zhu, Z., & Woodcock, C. E. (2012). Object-based cloud and cloud shadow detection in Landsat

808 imagery. *Remote Sensing of Environment*, 118, 83–94.

809 <https://doi.org/10.1016/j.rse.2011.10.028>

810

811 **List of Figure Captions**

812 Fig. 1. Land use and land cover in the Sacramento Valley, within California's Central Valley.
813 (Herbaceous wetlands and agriculture: National Land Cover Database (Homer et al., 2015);
814 flood-irrigated rice: (USDA-NASS, 2014).

815

816 Fig. 2. Landsat surface reflectance data availability (A) and quality (clear fraction identified by
817 the CFmask surface reflectance product) (B) for the Sacramento Valley (WRS-2 path 44/row 33)
818 from February to May, 1983-2015.

819

820 Fig. 3. Example of inverse distance weighted interpolation, guided by land survey boundaries
821 (California Department of Water Resources, 2016b) applied to classifications of SLC-off
822 Landsat 7 imagery.

823

824 Fig.4. Receiver operating characteristic (ROC) curves summarizing nine-fold cross validation of
825 water/non-water random forest models used to identify a spring mid-infrared surface reflectance
826 threshold. Dotted lines indicate ROC curves for each fold of the cross validation. The colored
827 line is the average ROC curve; cutoffs for the probability of membership in the water class from
828 0 to 1 in increments of 0.1 are shown with error bars indicating 95% confidence intervals for the
829 true positive rate and false positive rate at each cutoff.

830

831 Fig. 5. Long-term spring water extent trends from 1983 – 2015 in the Sacramento Valley of
832 California. Significant trends (linear regression, $p < 0.05$) are indicated by a solid line with the
833 equation shown, while non-significant trends are indicated by dashed lines. A significant
834 decrease in water extent in the Sacramento Valley was observed in late March, while a
835 significant increase in water extent was observed in late May.

836

837 Fig.6. Spring water extent and variability by two-week period in the Sacramento Valley from
838 1983 – 2015. Boxplots indicate the weighted mean extent and standard deviation of all open
839 water in the valley, as well as water detected within agriculture and herbaceous wetlands for each
840 two-week period in spring. The clear fraction of each Landsat image was used to weight
841 observations.

842

843 Fig. 7. Water extent and frequency for spring months in the Sacramento Valley from 1983-2015.
844 Example minimum (top row) and maximum (middle row) water/non-water classifications for
845 each month illustrate the variability of water extent in the study area; the year of each example
846 classification is indicated at the top left of each panel. The frequency of water detection (bottom
847 row) was calculated as the number of times water was identified in each pixel from a stack of all
848 water/non-water classifications for each month from 1983-2015, corrected by the total number of
849 cloud-free instances.

850

851 Fig. 8. Relativized estimates of spring water frequency within flood-irrigated agriculture (A) and
852 herbaceous wetlands (B) in the Sacramento Valley from 1983-2015. Water/non-water

853 classifications were combined for each two-week spring period and the per pixel frequency of
854 water detection was calculated, corrected by the total number of cloud-free instances within each
855 habitat type.

856

857 Fig. 9. Annual water availability compared to spring water extent in flood-irrigated agriculture
858 and herbaceous wetlands in the Sacramento Valley of California from 1983 – 2015. The Water
859 Year Index for the Sacramento River Basin scales annual water availability and designates each
860 year as either ‘Critical’ (≤ 5.4), ‘Dry’, ‘Below Normal’, ‘Above Normal’, or ‘Wet’ (≥ 9.2)
861 (California Department of Water Resources, 2016a). Herbaceous wetland water extent was
862 significantly correlated with the Water Year Index in all spring months; while the relationship
863 was only significant for agricultural water extent in March and April (equations shown for $p <$
864 0.05).